Edinburgh Research Explorer

Friction Coefficients for Droplets on Solids: The Liquid-Solid Amontons' Laws

Friction Coefficients for Droplets on Solids: The Liquid-Solid Amontons' Laws

Glen McHale[a*], Nan Gao[b], Gary G. Wells[a], Hernán Barrio-Zhang[a] and Rodrigo Ledesma-Aguilar[a]

[a]Institute for Multiscale Thermofluids, School of Engineering, The University of Edinburgh, Edinburgh EH9 3FB, UK.

[b]Department of Mechanical Engineering, University of Birmingham, Birmingham B15 2TT, UK

*Email: glen.mchale@ed.ac.uk

ABSTRACT

The empirical laws of dry friction between two solid bodies date back to the work of Amontons in 1699 and are pre-dated by the work of Leonardo da Vinci. Fundamental to those laws are the concepts of static and kinetic coefficients of friction relating the pinning and sliding friction forces along a surface to the normal load force. For liquids on solid surfaces contact lines also experience pinning and the language of friction is used when droplets are in motion. However, it is only recently that the concept of coefficients of friction has been defined in this context and that droplet friction has been discussed as having a static and a kinetic regime. Here we use surface free energy considerations to show the frictional force per unit length of a contact line is directly proportional to the normal component of the surface tension force. We define coefficients of friction for both contact lines and droplets, and provide a droplet analogy of Amontons' first and second laws, but with the normal load force of a solid replaced by the normal surface tension force of a liquid. In the static regime, the coefficient of static friction, defined by the maximum pinning force of a droplet, is proportional to the contact angle hysteresis, whereas in the kinetic regime the coefficient of kinetic friction is proportional to the difference in dynamic advancing and receding contact angles. We show the consistency between the droplet form of Amontons' first and second laws and an equation derived by Furmidge. We use these liquid-solid Amontons' laws to describe literature data, and report friction coefficients for various liquid-solid systems. The conceptual framework reported here should provide insight into the design of superhydrophobic, slippery liquid infused porous surfaces (SLIPS) and other surfaces designed to control droplet motion.

Keywords: Amontons' laws, Furmidge, coefficients of friction, droplets, SLIPS, lubricant impregnated surface, contact angle, contact angle hysteresis, Young's Law.

INTRODUCTION

Amontons' first two laws of dry friction state that for any two solid materials the lateral friction force, F_f, is directly proportional to the normal applied load, F_N, with a constant of proportionality, the friction coefficient μ, that is independent of the contact area (Figure 1a), i.e.

$$F_f = \mu F_N \qquad (1)$$

In the static regime the maximum frictional force prior to motion is characterised by a coefficient of static friction, μ_s, that is larger than the coefficient of kinetic friction, μ_k, in the sliding regime.[1–5] A third law attributed to Coulomb[6,7] further states that the coefficient of kinetic friction is independent of sliding velocity, although this is not generally obeyed at higher speeds. Whilst there are limits to the validity of these empirical laws they, nonetheless, provide a reference point for the dry friction of one solid sliding on a second solid. The language of friction is also very common when dealing with the motion of a droplet on a solid surface where there is a threshold pinning force and resistance to motion once the droplet is in motion. Overcoming the droplet pinning force has motivated the development of the fields of superhydrophobicity[8] and, more recently, lubricant impregnated/liquid infused surfaces (LIS) and slippery liquid infused porous surfaces (SLIPS).[9,10] Understanding low friction droplet motion has been a recent focus in droplet work.[11] Recently, combined measurements of the resistance force to the movement of a droplet on a range of solid substrates and their geometric shape parameters (front and back contact angles, contact length, contact width) have been reported.[12] The authors concluded the in-plane frictional force between a liquid drop and a solid can be divided into a static and a kinetic regime in a similar manner to the dry friction of solids. In a separate work, Barrio-Zhang *et al.*[13] suggested a direct droplet on solid analogy to eq 1 for the pinning force on a droplet through the use of the normal component of the surface tension force and the contact angle hysteresis. Their approach allows coefficients of static and kinetic friction to be defined for droplets.[11]

In his original work on resistance to droplet motion reported in 1962, Furmidge derived a widely used equation by considering the work done per unit area, $\gamma_{LV}(1+\cos\theta)$, in advancing a leading edge and dewetting the trailing edge of a droplet.[14] His work is often reported as

$$F_p = kw\gamma_{LV}(\cos\theta_B - \cos\theta_F) \qquad (2)$$

where F_p is the lateral (in-plane) force resisting motion, w is the droplet contact width and θ_F and θ_B are the contact angles at the front and rear (back) of the droplet and $k=1$ (see also references[15–18]). As discussed by Krasovitsky & Marmur[19], on an inclined plane θ_F and θ_B are the contact angles at the stability limits of the respective edges of the droplet, which do not in general simultaneously equal the advancing and receding contact angles although this is often assumed. In general, k is a dimensionless shape factor for the three phase contact line for which various authors have derived different values, e.g. $\pi/4$, $2/\pi$ and $24/\pi^3$ (see e.g. references[3,20]). Presented in this form, the resistive force can be

interpreted as the difference in the in-plane components of the surface tension forces at the front and rear of a droplet per unit length multiplied by the droplet perimeter length scaled by a shape factor k/π to account for the difference between a two-dimensional (2D) model and a three-dimensional (3D) droplet. Any dependence of eq 2 on the theoretical equilibrium Young's equation contact angle, θ_e, given by

$$\cos\theta_e = \frac{(\gamma_{SV} - \gamma_{SL})}{\gamma_{LV}} \tag{3}$$

is implicit. However, since the contact angle given by eq 3 must lie between the receding and advancing contact angles, it seems clear that there should be such a dependence. Recently, we argued that an analogy to coefficients of dry friction for solids can be obtained by a Taylor expansion of eq. 2 about an average value, assumed to be θ_e. To first order, this gives (Figure 1b)[11,13]

$$F_p = kw\gamma_{LV}\sin\theta_e(\theta_F - \theta_B) = \mu F_N \tag{4}$$

where the normal component of the interfacial tension force is

$$F_N = \pi w\gamma_{LV}\sin\theta_e \tag{5}$$

and the coefficient of droplet friction is defined by

$$\mu = \frac{k(\theta_F - \theta_B)}{\pi} = \frac{k\Delta\theta}{\pi} \tag{6}$$

In this formulation, the relation $F_p = \mu F_N$, is analogous to Amontons' first two laws of dry friction for solids, eq 1, but with the normal load force due to gravity replaced by the magnitude of the normal force due to the vertical component of surface tension (Figure 1c). An interesting difference is that for solid friction the reaction of the surface is to support the load of the solid and is therefore compressive, whereas in the droplet case the reaction is adhesive and is therefore tensile.
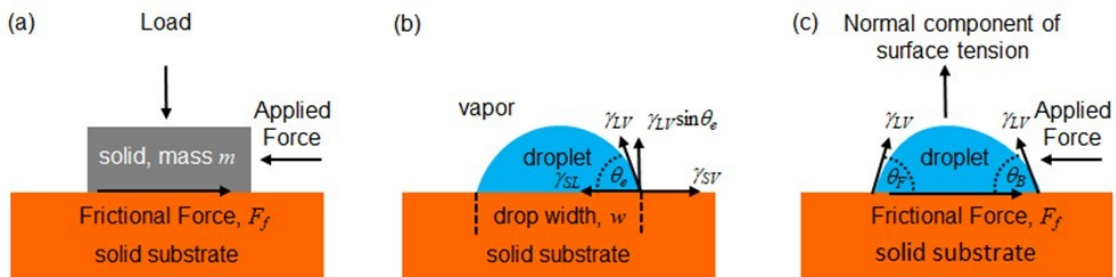
Figure 1. Amontons laws of friction: (a) Solid sliding on a solid due to an applied force. b) Droplet equilibrium without an applied force. (c) Droplet sliding/rolling on a solid due to an applied force.

The contact angle hysteresis, $\Delta\theta_{CAH} = \theta_A - \theta_R$, determined by using volume addition and withdrawal to measure the advancing contact angle, θ_A, and receding contact angle, θ_R, gives the maximum range of contact angles in the static regime and, hence, the coefficient of static friction, $\mu_s = k\Delta\theta_{CAH}/\pi$, at the onset of droplet motion. The difference in dynamic advancing contact angle at the front, $\theta_A(v)$, and the

dynamic receding contact angle at the rear, $\theta_R(v)$, of the droplet, $\Delta\theta(v)=\theta_A(v)-\theta_R(v)$, gives the coefficient of kinetic friction, $\mu_k=k\Delta\theta(v)/\pi$, for droplet motion and is potentially dependent on the droplet speed, v. The advantage of eq 4 to express eq. 2 is that it makes explicit the relationship between the in-plane frictional force and both the normal component of the surface tension force and the equilibrium contact angle. It also emphasizes the analogy to Amontons' first two laws for dry solid friction.

In this work, we show how a surface free energy approach can be used to derive an equation for advancing and receding contact line motion analogous to eq 4 (Amontons-like equation). For droplets, we show this leads to eq 4. This enables coefficients of static and kinetic friction to be defined using the contact angle hysteresis and dynamic contact angles. We show that our Amontons-like equation can accurately describe recent literature data on direct measurements of frictional forces using the complementary measurements of the droplet geometric parameters (front and back contact angles, width and length) and report the friction coefficients of droplets on surfaces for various liquid-solid systems. We also discuss how Amontons' second law interpreted as the statement that the coefficients of friction are independent of contact area can be applied to contact line motion, droplet motion and dry friction for motion of solids. Finally, we note that a dynamic contact angle in the Amontons-like equation suggests the frictional force in the kinetic regime is insensitive to droplet speed for low speeds (low capillary number) but at higher speeds (high capillary numbers) will increase.

SURFACE FREE ENERGY AND COEFFICIENTS OF FRICTION

Contact Lines

To further understand how an Amontons-like equation can arise for droplets, we consider changes in surface free energy for small advancing or receding displacements of a contact line. These arguments apply to 2D droplets and because they are local to the contact line do not depend on the precise profile of the droplet, e.g. whether it is gravitationally flattened or not. A small translation, Δr, of a contact line interchanges solid-vapor, $\gamma_{SV}\Delta r$, and solid-liquid, $\gamma_{SL}\Delta r$, interfacial energy and increases (or decreases if $\Delta r<0$) the liquid-vapor interfacial energy by $\gamma_{LV}\Delta r\cos\theta$. The first order change in the surface free energy, ΔE_{2D}, as a contact line is perturbed from its local contact angle, θ, is therefore

$$\Delta E_{2D} = (\gamma_{SL} - \gamma_{SV})\Delta r + \gamma_{LV}\Delta r\cos\theta \tag{7}$$

By requiring this change to vanish one obtains Young's law as the equilibrium contact angle, i.e. eq 3.

We now consider an advancing contact line and define an advancing contact angle θ_A (Figure 2a), with a difference from equilibrium, $\Delta\theta_A=\theta_A-\theta_e$, so that eq 7 becomes

$$\Delta E_A = (\gamma_{SL} - \gamma_{SV})\Delta r + \gamma_{LV}\Delta r\cos(\theta_e + \Delta\theta_A) \tag{8}$$

This can be expanded as

$$\Delta E_A \approx (\gamma_{SL} - \gamma_{SV})\Delta r + \gamma_{LV}\Delta r[\cos\theta_e - \Delta\theta_A\sin\theta_e] \tag{9}$$

Using Young's equation (eq 3), and recognising that the equilibrium normal component of the liquid-vapor interfacial tension force per unit length of the contact line is $f_N = \gamma_{LV} \sin \theta_e$, we find

$$\Delta E_A \approx -\Delta r \Delta \theta_A f_N \qquad (10)$$

Similarly, we consider a receding contact angle θ_R (Figure 2b), and define the difference, $\Delta \theta_R = \theta_e - \theta_R$, we obtain

$$\Delta E_R = (\gamma_{SV} - \gamma_{SL}) \Delta r - \gamma_{LV} \Delta r \cos(\theta_e - \Delta \theta_R) \qquad (11)$$

and so

$$\Delta E_R \approx -\Delta r \Delta \theta_R f_N \qquad (12)$$

Because the changes in surface energy given by eq 10 and eq 12 are the result of displacements, the corresponding external forces needed to cause such displacements, per unit length of the contact line, are $\Delta \theta_A f_N$ and $\Delta \theta_R f_N$. We therefore define coefficients of friction for the advancing and receding contact lines as $\mu_A = \Delta \theta_A$ and $\mu_R = \Delta \theta_R$.
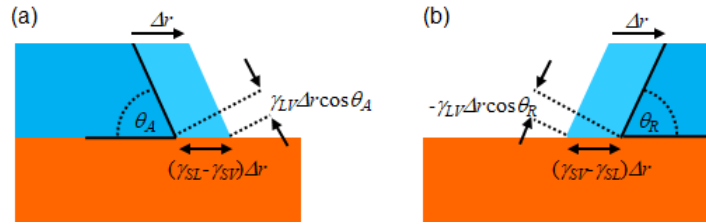

Figure 2. Surface free energy changes: (a) Advancing contact line. (b) Receding contact line.

Droplets

We now consider the advancing and receding contact lines at the front and back of a 2D droplet with contact angles θ_F and θ_B, respectively. In such a case, the leading edge of the droplet advances, while the trailing edge recedes. The energy change, ΔE_{2D}, in translating the position of the droplet by Δr is

$$\Delta E_{2D} \approx -\Delta r (\Delta \theta_F + \Delta \theta_B) f_N = -\Delta r \Delta \theta f_N \qquad (13)$$

where $\Delta \theta = \theta_F - \theta_B$ is either the contact angle hysteresis for a static droplet or the difference in dynamic contact angles at the front and back edges of a moving droplet.

We now consider a 3D droplet maintaining a circular contact with the solid. Around the front half of the droplet each point on the contact line advances along the direction of motion (x-direction) by the same amount Δx. Similarly, around the back half of the droplet each point on the contact line recedes along the direction of motion by the same absolute amount. The liquid-solid and solid-vapor area changes in the vicinity of the contact line are given by integrating $r \cos \varphi d\varphi$, where $r = w/2$ is the contact radius and φ is the in-plane polar angle, around the front (or back) half-perimeter and this causes a

change in the liquid-vapor interfacial energy of $2r\Delta x\gamma_{LV}\cos\theta_F$ (or $2r\Delta x\gamma_{LV}\cos\theta_B$). The total change in surface free energy is

$$\Delta E_{3D} \approx -\Delta x(\Delta\theta_F + \Delta\theta_B)2rf_N = -\Delta x\left(\frac{\Delta\theta}{\pi}\right)F_N \tag{14}$$

where $F_N = 2\pi r\gamma_{LV}\sin\theta_e$ is the total normal component of the liquid-vapor interfacial tension force around the droplet contact line. Equation 14 suggests the total frictional force is proportional to the total normal force with a coefficient of proportionality (coefficient of droplet friction) $\mu = \Delta\theta/\pi$, i.e. $F_P = \mu F_N$. This is consistent with eq 6 using $k=1$ derived from Furmidge's original formulation (eq. 2) using a Taylor series expansion.

Generally, we expect the advancing and receding contact angles (or more accurately the cosines) to depend on position around the droplet perimeter and, once motion begins the droplet to elongate rather than maintaining a circular contact area, and so introduce an overall constant k. The resulting coefficient of static friction for a droplet is therefore

$$\mu_s = k\Delta\theta_{CAH}/\pi \tag{15}$$

When a droplet is in motion travelling at a speed, v, there will be different dynamic contact angles at the front (advancing) contact line, $\theta_A(v)$, and at the back (receding) contact line, $\theta_R(v)$. This leads to the concepts of dynamic advancing and receding coefficients of kinetic friction based upon the dynamic advancing, receding and equilibrium contact angles. By defining a normal force, $F_N = \pi w\gamma_{LV}\sin\theta_e(v)$, and a difference in dynamic advancing and receding contact angles, $\Delta\theta(v) = \theta_A(v) - \theta_R(v)$, we find a kinetic coefficient of droplet friction, μ_k,

$$\mu_k = k\Delta\theta(v)/\pi \tag{16}$$

COMPARISON TO LITERATURE DATA

To consider the accuracy of our Amontons-like equation for droplets we can consider whether the geometric parameters measured optically are consistent with direct measurements of in-plane friction forces. A set of data, which is ideal for this purpose, was produced by Gao *et al* who reported measurements of the force imparted on a cantilever by a droplet on a moving solid plane.[12] They used two cameras to simultaneously view the droplet in side profile and parallel to the motion thereby allowing the geometric parameters of front and back contact angles, and droplet contact length and contact width to be measured. Their experiments used droplets of water, hexadecane and 1-butyl-2,3-dimethylimidazolium bis(trifluoromethanesulfonyl)imide. They used 1H,1H,2H,2H-perfluorodecyltrichlorosilane (PFDTS, 96%) to create fluorinated surfaces from silicon wafers, silicone nanofilaments and SU-8 micropillars (25 μm high, with 50×50 μm^2 top areas and pillar–pillar distance between centres of two adjacent pillars of 100 μm). To create fluorinated TiO2 nanoparticle surfaces they used 1H,1H,2H,2H-perfluorooctyltrichlorosilane (PFOTS, 97%). They also used cross-linked

PDMS and liquid-like PDMS[21] surfaces. Full details of their materials and methods are given in the on-line version of their paper.[12]

We start by analysing the data from their supplementary information for droplets of water on fluorinated silicon (Water/PFDTS-Si), superhydrophobic fluorinated silicone nanofilaments (Water/PFDTS-Si-nF), fluorinated SU-8 micropillars (Water/PFDTS-SU8-µP), fluorinated TiO_2 nanoparticles (Water/PFOTS-TiO_2-nP) and PDMS (Water/PDMS), and for droplets of hexadecane on fluorinated silicone (Hexadecane/PFDTS-Si) (i.e. Figure S5, S6, S8-S10 and S7 in their supplementary information). In each case the substrates were translated at a constant speed of approximately 200 µm/s. The surface tension of water and hexadecane are γ_{LV}=72.8 mN/m and 27.5 mN/m, respectively. The droplets initially have similar contact length, l, and contact width, w, but as a droplet is forced into motion its length can become up to 20% larger than its width. In our theory we have generally assumed a circular contact area whereas droplets in motion can have a significantly elongated droplet-solid contact shape. Here, we assume the contact width and length define an ellipse and use Ramanujan's formula[22,23] to calculate an approximate equivalent circular contact diameter, w_{eqiv}, with the same perimeter length

$$w_{eqiv} = (l + w)\left[1 + \frac{3h}{10+\sqrt{4-3h}}\right] \tag{17}$$

where $h=(l-w)^2/(l+w)^2$. We then use an average of the front and rear forces to estimate the average normal component of surface tension force per unit length along the droplet perimeter

$$\gamma_{LV}\sin\theta_e = \gamma_{LV}(\sin\theta_F + \sin\theta_B)/2 \tag{18}$$

Figure 3 shows the experimentally measured frictional force data as a solid line. The optically measured contact angles at the front and rear of the droplet, and the droplet contact length and width data are used in eq 4 give the solid symbols (●●●). For these data points a value of k=1.32 has been used in all data sets apart from Water/PDMS where a value of k=1.04 has been used, to match to the measured frictional force during steady droplet motion towards the end of each time sequence. In all six cases, eq 4 captures the shape of the frictional force with time, but in three cases the calculated force systematically overestimates the measured value in the static regime below the peak in the force. The most obvious example is for Water/PFDTS-SU8-µP where at time t=0 the calculated force is clearly offset from the measured force (Figure 3d).

To match up each time sequence we therefore assume a small time offset between the frictional force and the estimates from eq 4 using the optical geometric measurements. These offset time data sequences are shown by the open symbols (○○○) in figure 3 and correspond to offsets of between -0.4s and 1.5s (Note that for Water/PFDTS-Si-nF the solid symbols overlay and obscure the open symbols because no offset was required). In the case of Water/PDMS where a lower value of k=1.04 was required to match the kinetic regime, the peak in the force curve separating the static and kinetic regimes is more rounded and extended than in the other data sets. It appears likely both this feature and the lower value of k is

because of the softness of the PDMS substrate compared to the other substrates which are rigid. We conclude from these data sets that the droplet form of Amontons' laws (eq 4) is in excellent agreement with the experimental data provided one assumes a small offset in the time axes.
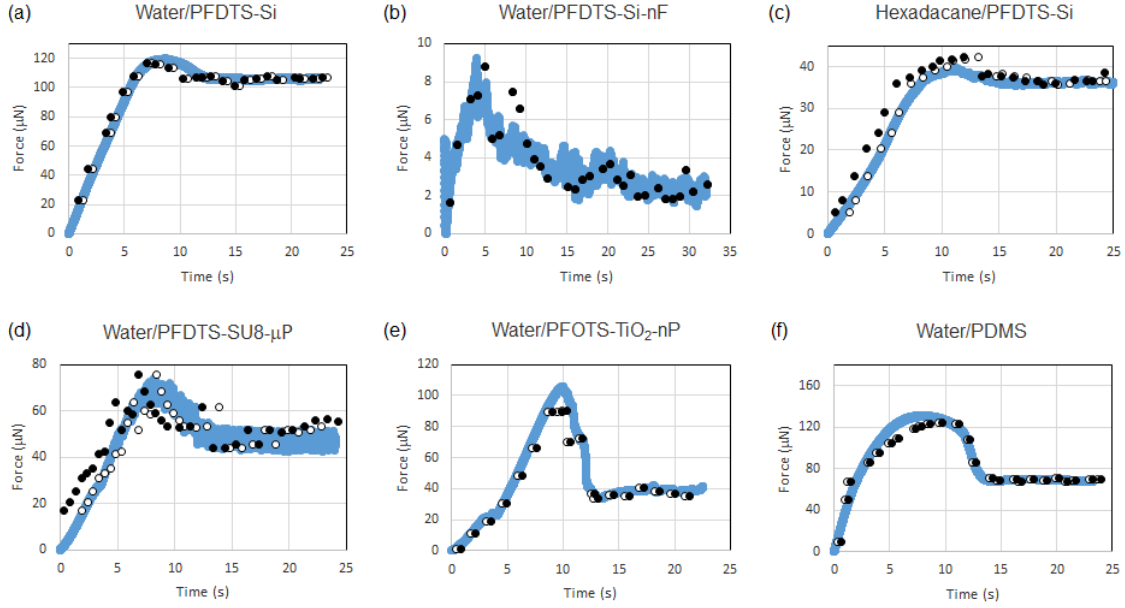

Figure 3. Comparison of the directly measured frictional force (solid line) and the frictional force deduced using the droplet Amontons laws (eq 4) and the measured geometric parameters from droplet images with $\mu=k\Delta\theta/\pi$ and $k=1.32$ for data in panels (a)-(e) and $k=1.04$ for data in panel (f). The solid symbols (●●●) are without offsets to the time axes and the open symbols (○○○) use offsets to the time axes of 0.45, 0.00, 1.20, 1.50, -0.4 and -0.3 for data in panels (a)-(f), respectively.

We now discuss possible causes of an offset in the time axes, which is required primarily to match the data in the early time static regime period in Figures 3c and 3d. The experimental method used two cameras to measure geometric parameters and also recorded the frictional force *via* the deflection of a hollow rectangle glass capillary inserted into the centre of the droplet. The matching of the three time series used the end of data capture for each run and so there is a possibility of slight mismatch. It is also possible that the distortion of the droplet shape or the methods to estimate contact angles in the static and dynamic regimes might cause offsets. In addition, when the stage is in motion the position of the capillary within the droplet moves during an initial period to the front edge of the droplet (the only exception is for the superhydrophobic case of Water/PFDTS-Si-nF); the change in relative position of the capillary in the droplet and the linked deformation of the liquid-vapor interface is visible in the supplementary videos provided with the published paper reporting the original data. The speed of translation of the substrates and the droplet spherical radius provide timescales larger than that needed for the offset in time axes in the fitting in Figure 3. This rearrangement of relative position of the capillary when measuring force is a complication not present in the analogous experiments of friction with a sliding solid. Whilst we cannot be certain for the cause of an offset in the time axes for the droplet experiments, it is plausible that offsets may be subtly within the experimental method.

In Figure 4 we show the time sequences for the coefficients of friction, $\mu = k\Delta\theta/\pi$, and the normal component of surface tension force, $F_N = \pi w_{eqiv}\gamma_{LV}\sin\theta_e$, corresponding to the data in Figure 3. From these plots we identify the maximum value during the initial increase in μ as the coefficient of static friction, μ_s, and the average value during steady state motion after the peak as the coefficient of kinetic friction, μ_k, (Table 1). Due to the time resolution in the measurement of the geometric parameters the data cannot capture narrow peaks and so we cannot provide an uncertainty estimate beyond noting the coefficient of static friction is likely to be an underestimate. In contrast, the coefficient of kinetic friction can be taken as an average over a period of time when it is approximately constant and this allows an estimate of its uncertainty. To place the magnitude of these coefficients of friction into the context of solids, the coefficient of friction for Teflon sliding on Teflon[24,25] is 0.05 and for Aluminium Magnesium Chloride (AlMgB$_{14}$) (also known as BAM), reported to be the world's slipperiest solid material, is 0.04-0.05 (unlubricated) in tests in diamond tip nano-scratch tests.[26]
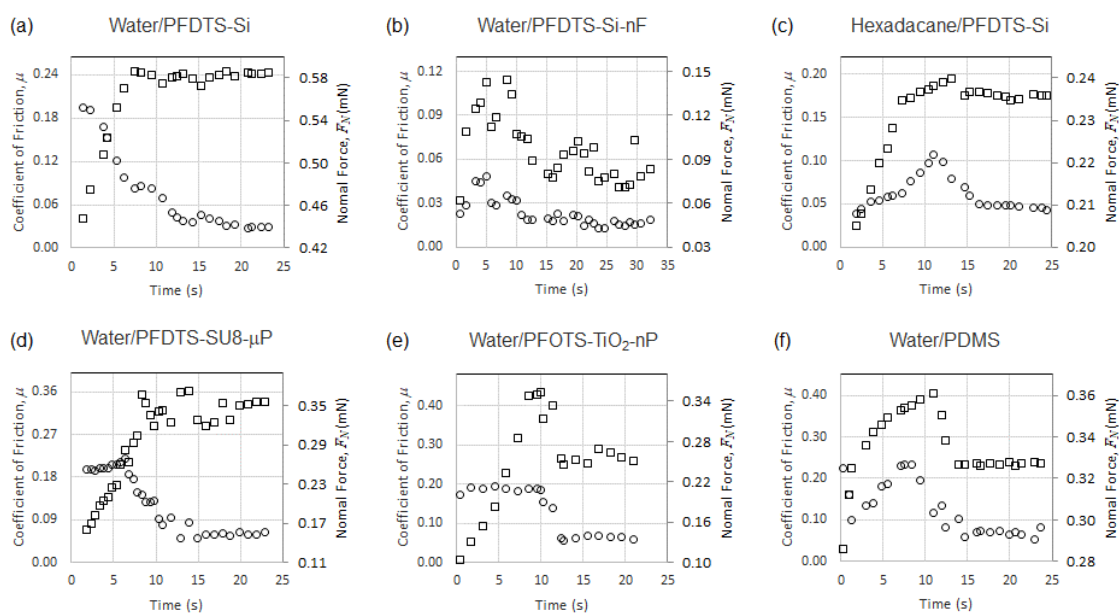

Figure 4. The coefficients of friction (□□□ symbols - left hand axes) and the normal component of the surface tension force (○○○ symbols - right hand axes) for the data in Figure 3.

Table 1. Coefficients of Static and Kinetic Friction for Various Droplet/Solid Systems

System	μ_s	μ_k
Water/PFDTS-Si	0.244	0.240±0.004
Water/PFDTS-Si-nF	0.114	0.056±0.014
Hexadecane/PFDTS-Si	0.196	0.176±0.006
Water/PFDTS-SU8-μP	0.362	0.340±0.040
Water/PFOTS-TiO$_2$-nP	0.428	0.266±0.016
Water/PDMS	0.404	0.236±0.002

In Figure 5 we reproduce the time sequences for the front and rear (back) contact angles corresponding to the data in Figure 3. Apart from water on PDMS, the front contact angle always increases to a maximum and then stabilizes rather than decreasing in the kinetic regime (to within the measurement accuracy). In contrast the rear contact angle decreases and either stabilizes or increases before stabilizing in the kinetic regime. The difference between the static and kinetic coefficient of friction, where there is one, is therefore determined by the contact line motion at the back of the droplet. To quote Extrand and Gent "*Simultaneously, the front edge of the drop tends to creep forward slightly, increasing the length of the drop. But the entire drop does not move until a critical force F is applied*".[20] The difference in motion of the advancing and receding contact lines of a droplet on surfaces has been discussed by a range of authors (e.g. references[19,21,27–30]). For example, one difference for the receding contact line on a micropillar superhydrophobic surface compared to the advancing contact line is that it can dewet a micropillar by the formation and rupture of a capillary bridge,[31] which is also a mechanism that is applicable to other types of pinning features on surfaces. It is further known that droplets break at the rear contact line upon advancing when the receding contact angle approaches zero.[20]
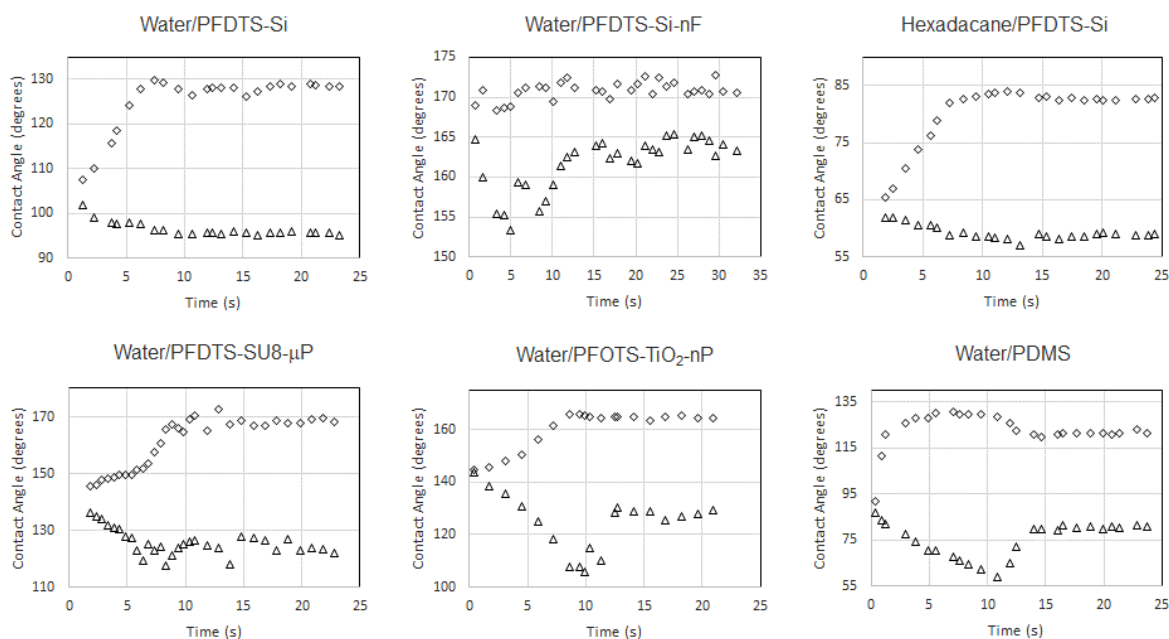

Figure 5. The front contact angle (◊◊◊ symbols) and rear contact angle (ΔΔΔ symbols) for the data in Figure 3.

Gao *et al.*[12] also considered the frictional forces on an ionic liquid (1-butyl-2,3-dimethylimidazoliumbis(trifluoromethanesulfonyl)imide) with a surface tension of γ_{LV}=34.6m N/m on a fluorinated silicon (IL-PFDTS-Si) substrate translated at a constant linear velocity of approximately 200 μm/s. To fit the data for the kinetic regime requires k=1.13 (solid symbols ••• in Figure 6a) with an offset to the time axes of 0.6 to bring the majority of the static regime data into agreement (open symbols ∘∘∘ in Figure 6a). Fitting this data assuming k=1.32 to be consistent with the five data sets in

Figure 3 for droplets on rigid substrates overestimates the force in the kinetic regime and would require an offset of c.a. 5 µN to overlay the majority of the data with the exception of the data in the peak region. The data for the front and rear (back) contact angles of the droplet shows the behaviour of the rear contact angle differs from other data sets in this peak region (Figure 6b) with a step decrease of around 10° occurring after 7 s and before the peak force at c.a. 10 s. This suggests this experiment might have been influenced by some pinning defects on this particular sample.
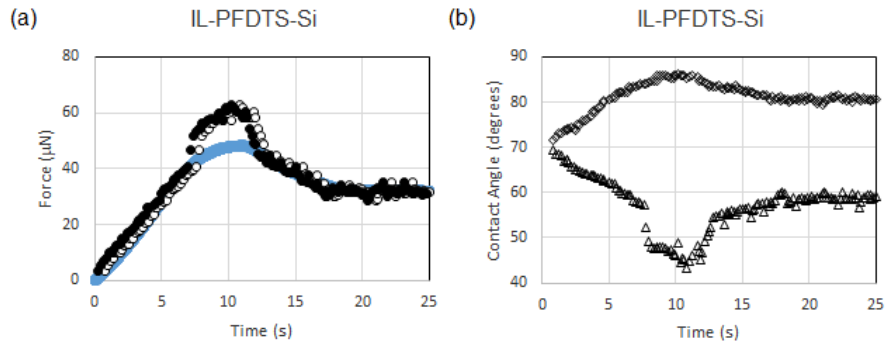

Figure 6. Ionic liquid on fluorinated silicon (IL-PFDTS-Si): (a) Comparison of the measured frictional force (solid line) to the force deduced from geometric parameters with $k=1.13$ without offsets (●●● symbols) and with an offset to the time axes of 0.6 s (○○○ symbols). (b) Front contact angle (◊◊◊ symbols) and rear contact angle (ΔΔΔ symbols).

Gao *et al.*[12] measured the friction force as a function of time for a c.a. 1.0 µl droplet of water on liquid-like PDMS where, unlike other surfaces, the maximum frictional force and the frictional force during steady motion (251 µm/s) were found to be equal. However, their data does not include any of the droplet geometric measurements (front and back contact angles, contact width and contact length). These "liquid-like' PDMS samples were prepared following the method reported by Krumpfer and McCarthy.[21] In these surfaces only one end of the PDMS is covalently grafted on the substrate with the remaining part of the PDMS keeping its high mobility with rotational and/or bending motion. Using the information in Pilat *et al.*[32] we can estimate the advancing and receding contact angles for water on these surfaces $\theta_A=105\pm2°$ and $\theta_R=93\pm3°$ using the volume addition and withdrawal method and so the contact angle hysteresis is $\Delta\theta_{CAH}=12\pm5°$. By assuming the droplet is approximately a spherical cap shape we can estimate the contact width from the droplet volume and an average equilibrium contact angle. This allows us to estimate the frictional force from eq 4 using $k=1.32$ is (14 ± 6) µN, consistent to within error of the measured friction force of 15.1 µN in the kinetic regime. This also implies a static coefficient of friction for this liquid-like surface of $\mu_s=0.09\pm0.04$. A single universal value of $k=1.32$ therefore appears to be consistent with the data in Figure 3 from Gao *et al.*[12] for the five rigid substrates provided one allows for an offset in the time axes.

Wang & McCarthy[33] also reported an alternative slippery omniphobic covalently attached liquid (SOCAL) surface obtained through acid- catalyzedgraft polycondensation of dimethyldimethoxysilane with extremely low CAH ($\leq 1°$) for liquids that span surface tensions from 78.2 to 18.4 m/Nm (for a discussion of the liquid-like nature of surface-tethered PDMS brushes see ref.[34]). Using k=1.32, their paper implies coefficients of static friction of μ_s=0.007, 0.001, 0.003, 0.001, <0.001 and <0.001 for water, diiodomethane, touene, hexadecane, cyclohexane, decane and hexane, respectively. Measurements reported by Barrio-Zhang *et al.*[33] for water on SOCAL report a contact angle hysteresis of $\Delta\theta_{CAH}$=2.5±1.7° giving an estimated coefficient of static friction of μ_s=0.018±0.012. Such low coefficients are comparable or lower than the coefficients of static friction reported for the most slippery solid-on-solid systems (i.e. Teflon and BAM).

DISCUSSION OF AMONTONS' LAWS IN A DROPLET CONTEXT

Gao *et al.*[2] provide a historical review of Amontons' laws from studies of the force required to slide a solid object on a solid surface starting with the conclusions of Leonardo da Vinci that the friction force doubled when the weight (normal externally applied load, F_N) was doubled and, second, that the (lateral) friction force, F, was independent of the way the objects were positioned on the surface (i.e., that the force did not depend on the area of contact, A, between the moving surfaces). They note that these observations were later confirmed by Amontons (1663-1706), and that Coulomb further noted the velocity independence of the friction force. Mathematically, this is summarized as a friction coefficient, μ=F/F_N which is independent of the "apparent" or macroscopic contact area and sliding velocity of the load.

A striking visual demonstration of Amontons' second law is to use a solid block with one face much smaller than the other and show the friction force is independent of whether it is placed on its largest or smallest surface area face. In the droplet case, because the material is a liquid, one cannot change the contact area between the droplet and the solid in such a manner. To change the area one would need to change the droplet volume or the equilibrium contact angle (through either the surface chemistry or roughness/topography). As stated above, da Vinci's second observation cannot be applied to droplet friction. However, it remains the case that one can state that for a droplet on a solid the (lateral) friction force is directly proportional to the normal component of surface tension force (First law) with a constant of proportionality, the coefficient of friction, that is constant and independent of the contact area (Second law). A key part of this statement is that it is the coefficient of friction, μ, which is independent of contact area and this does not include statements about the orientation of a rigid object.

In considering the droplet form of Amontons' third/Coulombs law, eq 4 provides insight beyond eq. 2 derived by Furmidge. Specifically, it provides an explicit dependence on the contact angle through the normal component of the surface tension force and is in a separable form with a contact angle hysteresis factor. From the perspective of designing a superhydrophobic surface, eq. 4 encapsulates the

idea that a surface with a high equilibrium angle will give a low normal component of the surface tension force, but the contact angle hysteresis will determine the coefficient of static friction and whether it is a so-called "sticky" or "slippery" superhydrophobic surface. From the perspective of designing lubricant impregnated or slippery liquid infused porous surfaces, eq. 4 encapsulates the idea that a sufficiently low contact angle hysteresis will give a low coefficient of static friction. On these surfaces drop motion can be easily initiated, without the need for high equilibrium contact angles to achieve a low normal component of the surface tension force. The recognition that the coefficient of kinetic friction can be different to the coefficient of static friction is a reminder that designing a surface on which droplet motion can be easily initiated may not be the same as designing a surface that has dynamic drop mobility. This appears relevant to liquid-like surfaces, such as SOCAL.

One can also hypothesize that the normal component of surface tension force should use the dynamic contact angle, θ_D(Ca), which in the Cox-Voinov theory[35,36] is predicted as a function of the speed of the contact line, U, by

$$\theta_D^3 = \theta_m^3 + 9\text{Ca} \log_e \left(\frac{L}{l_m} \right) \tag{19}$$

where Ca= $\eta U / \gamma_{LV}$ is the capillary number and η is the viscosity of the droplet. For an advancing contact line we assume that the microscopic contact angle is $\theta_m = \theta_A$. For a receding contact line, eq 19 is also valid[36] where we assume $\theta_m = \theta_R$ and let Ca$\rightarrow$ –Ca. In eq 19, the logarithmic term uses a microscopic length l_m and a typical macroscopic length scale at which the dynamic contact angle is measured.[37] For small droplets, L is often taken as the capillary length $l_c = (\gamma_{LV}/\rho g)^{1/2}$ where ρ is the density of the droplet and g=9.81 m/s^2 is the acceleration due to gravity. Equation 19 suggests a low-speed regime where the dynamic contact angle remains approximately constant, i.e. when $|\text{Ca}| \ll \theta_m^3/9\log_e(L/l_m)$. Beyond this limit, the dynamic contributon in equation 19 can be used to estimate the kinetic coefficient of friction. Using a Taylor expansion around Ca=0, we expect the frictional coefficient arising from Cox-Voinov theory to vary linearly with the interface speed to first order, i.e.

$$\mu_k = \frac{k}{\pi} \left(\Delta\theta + \frac{6\text{Ca}}{\theta_e^2} \log_e \left(\frac{L}{l_m} \right) \right) \tag{20}$$

We hope that such considerations on the possible velocity dependence of the coefficient of kinetic friction will provide motivation for future experiments to simultaneously measure the friction force and the geometric parameters of the droplet, particularly in the kinetic regime.

Beyond droplets, it is possible that our ideas on the coefficient of friction for advancing and receding contact lines will be relevant to consideration of liquid friction on the microscale, for example, in the context of the Molecular Kinetic Theory[38,39], and to molecular dynamics simulations of wetting[40,41]. We believe there will also be broader relevance to macroscopic processes and other systems, e.g. porous media and capillary imbibition[42]. Our work does not address microscopic models, such as the Prandlt-

Tomlinson model[43–46], which might provide a complementary approach to friction on rough/textured and chemically heterogeneous surfaces where capillary bridges may form and break as the droplet dewets successive features.[31,47,48]

CONCLUSION

In this work, we have developed the concept of coefficients of static and kinetic friction for contact lines and droplets. We have shown that a surface free energy approach can produce an equation and laws analogous to Amontons' first and second laws of dry solid friction with the in-plane frictional force proportional to the normal component of the surface tension force and a constant of proportionality $k\Delta\theta/\pi$. We have shown these laws are consistent with eq. 2 relating advancing and receding contact angles to the pinning force on a droplet. We have compared the prediction of these new liquid-solid Amontons-like laws against recent experimental measurements, reporting for the first time the friction coefficients of droplets on surfaces for various liquid-solid systems. We have also suggested that Amontons' third law/Coulombs law may be considered within a model of coefficient of kinetic friction and dynamic contact angles. Our work provides a conceptual framework linking droplet and contact line friction to solid on solid friction and provides a unified approach to considering Furmidge's equation for droplet pinning and droplet friction.

ACKNOWLEDGEMENTS

REFERENCES

(1)   Amonton, G. De La Resistance Cause'e Dans Les Machines (About Resistance and Force in Machines). *Mémoires l'Académie R.* **1699**, 257–282.

(2)   Gao, J.; Luedtke, W. D.; Gourdon, D.; Ruths, M.; Israelachvili, J. N.; Landman, U. Frictional Forces and Amontons' Law: From the Molecular to the Macroscopic Scale. *J. Phys. Chem. B* **2004**, *108* (11), 3410–3425.

(3)   ElSherbini, A. I.; Jacobi, A. M. Retention Forces and Contact Angles for Critical Liquid Drops on Non-Horizontal Surfaces. *J. Colloid Interface Sci.* **2006**, *299* (2), 841–849.

(4)   Dowson, D. *History of Tribology*, 2nd ed.; Professional Engineering Publishing: London, 1998.

(5)   Popova, E.; Popov, V. L. The Research Works of Coulomb and Amontons and Generalized Laws of Friction. *Friction* **2015**, *3* (2), 183–190.

(6)   Coulomb, C. A. Essai Sur Une Application Des Regles de Maximis & Minimis a Quelques Problemes de Statique, Relatifs a l'architecture. *Mem. Math. l'Academie R. Sci. Paris* **1773**, *7*,

343–382.

(7)   Heyman, J. *Coulomb's Memoir on Statics : An Essay in the History of Civil Engineering*; Imperial College Press, 1998.

(8)   Quéré, D. Wetting and Roughness. *Annu. Rev. Mater. Res.* **2008**, *38* (1), 71–99.

(9)   Lafuma, A.; Quéré, D. Slippery Pre-Suffused Surfaces. *Epl* **2011**, *96* (5), 56001.

(10)   Wong, T.-S.; Kang, S. H.; Tang, S. K. Y. Y.; Smythe, E. J.; Hatton, B. D.; Grinthal, A.; Aizenberg, J. Bioinspired Self-Repairing Slippery Surfaces with Pressure-Stable Omniphobicity. *Nature* **2011**, *477* (7365), 443–447.

(11)   Hardt, S.; McHale, G. Flow and Drop Transport Along Liquid-Infused Surfaces. *Annu. Rev. Fluid Mech.* **2022**, *54* (1), 83–104.

(12)   Gao, N.; Geyer, F.; Pilat, D. W.; Wooh, S.; Vollmer, D.; Butt, H.; Berger, R. How Drops Start Sliding over Solid Surfaces. *Nat. Phys.* **2018**, *14* (2), 191–196.

(13)   Barrio-Zhang, H.; Ruiz-Gutiérrez, É.; Armstrong, S.; McHale, G.; Wells, G. G.; Ledesma-Aguilar, R. Contact-Angle Hysteresis and Contact-Line Friction on Slippery Liquid-like Surfaces. *Langmuir* **2020**, *36* (49), 15094–15101.

(14)   Furmidge, C. G. L. Studies at Phase Interfaces. 1. Sliding of Liquid Drops on Solid Surfaces and a Theory for Spray Retention. *J. Colloid Sci.* **1962**, *17*, 309–324.

(15)   Bikerman, J. J. On the Formation and Structure of Multilayers. *Proc. R. Soc. London. Ser. A. Math. Phys. Sci.* **1939**, *170* (940), 130–144.

(16)   Macdougall, G.; Ockrent, C. Surface Energy Relations in Liquid/Solid Systems I. The Adhesion of Liquids to Solids and a New Method of Determining the Surface Tension of Liquids. *Proc. R. Soc. London. Ser. A. Math. Phys. Sci.* **1942**, *180* (981), 151–173.

(17)   Frenkel, Y. I. On the Behavior of Liquid Drops on a Solid Surface. 1. The Sliding of Drops on an Inclined Surface. *J. Exptl. Theor. Phys.* **1948**, *18*, 659–668.

(18)   Kawasaki, K. Study of Wettability of Polymers by Sliding of Water Drop. *J. Colloid Sci.* **1960**, *15* (5), 402–407.

(19)   Krasovitski, B.; Marmur, A. Drops down the Hill: Theoretical Study of Limiting Contact Angles and the Hysteresis Range on a Tilted Plate. *Langmuir* **2005**, *21* (9), 3881–3885.

(20)   Extrand, C. W.; Gent, A. N. Retention of Liquid Drops by Solid Surfaces. *J. Colloid Interface Sci.* **1990**, *138* (2), 431–442.

(21)   Krumpfer, J. W.; McCarthy, T. J. Contact Angle Hysteresis: A Different View and a Trivial

Recipe for Low Hysteresis Hydrophobic Surfaces. *Faraday Discuss.* **2010**, *146*, 103–111.

(22)   *Ramanujan, S.: Notebooks*; Tata Institute of Fundamental Research, Bombay, 1957.

(23)   Tian, J. F.; Yang, Z.; Ha, M. H.; Xing, H. J. A Family of High Order Approximations of Ramanujan Type for Perimeter of an Ellipse. *Rev. la Real Acad. Ciencias Exactas, Fis. y Nat. - Ser. A Mat.* **2021**, *115* (2), 1–20.

(24)   Flom, D. G.; Porile, N. T. Friction of Teflon Sliding on Teflon. *J. Appl. Phys.* **1955**, *26* (9), 1088–1092.

(25)   Kuzharov, A. S. Polytetrafluoroethylene Fiber-Based Composite Antifriction Coatings. *Ind. Eng. Chem. Res.* **1993**, *32* (5), 763–773.

(26)   Tian, Y.; Bastawros, A. F.; Lo, C. C. H.; Constant, A. P.; Russell, A. M.; Cook, B. A. Superhard Self-Lubricating AlMgB14 Films for Microelectromechanical Devices. *Appl. Phys. Lett.* **2003**, *83* (14), 2781–2783.

(27)   Gao, L.; McCarthy, T. J. Contact Angle Hysteresis Explained. *Langmuir* **2006**, *22* (14), 6234–6237.

(28)   Wang, L.; McCarthy, T. J. Shear Distortion and Failure of Capillary Bridges. Wetting Information Beyond Contact Angle Analysis. *Langmuir* **2013**, *29* (25), 7776–7781.

(29)   Schellenberger, F.; Encinas, N.; Vollmer, D.; Butt, H. How Water Advances on Superhydrophobic Surfaces. *Phys. Rev. Lett.* **2016**, *116* (9), 096101.

(30)   Kusumaatmaja, H.; Yeomans, J. M. Modeling Contact Angle Hysteresis on Chemically Patterned and Superhydrophobic Surfaces. *Langmuir* **2007**, *23* (11), 6019–6032.

(31)   Krumpfer, J. W.; Bian, P.; Zheng, P.; Gao, L.; McCarthy, T. J. Contact Angle Hysteresis on Superhydrophobic Surfaces: An Ionic Liquid Probe Fluid Offers Mechanistic Insight. *Langmuir* **2011**, *27* (6), 2166–2169.

(32)   Pilat, D. W.; Papadopoulos, P.; Schäffel, D.; Vollmer, D.; Berger, R.; Butt, H. Dynamic Measurement of the Force Required to Move a Liquid Drop on a Solid Surface. *Langmuir* **2012**, *28* (49), 16812–16820.

(33)   Wang, L.; McCarthy, T. J. Covalently Attached Liquids: Instant Omniphobic Surfaces with Unprecedented Repellency. *Angew. Chemie Int. Ed.* **2016**, *55* (1), 244–248.

(34)   Zhao, X.; Khatir, B.; Mirshahidi, K.; Yu, K.; Kizhakkedathu, J. N.; Golovin, K. Macroscopic Evidence of the Liquidlike Nature of Nanoscale Polydimethylsiloxane Brushes. *ACS Nano* **2021**, *15* (8), 13559–13567.

(35)   Voinov, O. V. Hydrodynamics of Wetting. *Fluid Dyn.* **1977**, *11* (5), 714–721.

(36)   Cox, R. G. The Dynamics of the Spreading of Liquids on a Solid Surface. Part 1. Surfactants. *J. Fluid Mech.* **1986**, *168* (1), 169–194.

(37)   Bonn, D.; Eggers, J.; Indekeu, J.; Meunier, J.; Rolley, E. Wetting and Spreading. *Rev. Mod. Phys.* **2009**, *81* (2), 739–805.

(38)   Blake, T. D.; Haynes, J. M. Kinetics of Liquid Liquid Displacement. *J. Colloid Interface Sci.* **1969**, *30* (3), 421–423.

(39)   Blake, T. D. Dynamic Contact Angles and Wetting Kinetics. In *Wettability*; Berg, J. C., Ed.; Dekker: NewYork, 1993; pp 251–309.

(40)   Blake, T. D.; De Coninck, J. The Influence of Solid-Liquid Interactions on Dynamic Wetting. *Adv. Colloid Interface Sci.* **2002**, *96* (1–3), 21–36.

(41)   De Coninck, J.; Blake, T. D. Wetting and Molecular Dynamics Simulations of Simple Liquids. *Annu. Rev. Mater. Res.* **2008**, *38*, 1–22.

(42)   Martic, G.; Gentner, F.; Seveno, D.; Coulon, D.; De Coninck, J.; Blake, T. D. A Molecular Dynamics Simulation of Capillary Imbibition. *Langmuir* **2002**, *18* (21), 7971–7976.

(43)   Popov, V. L.; Gray, J. A. T. Prandtl-Tomlinson Model: History and Applications in Friction, Plasticity, and Nanotechnologies. *ZAMM - J. Appl. Math. Mech. / Zeitschrift für Angew. Math. und Mech.* **2012**, *92* (9), 683–708.

(44)   Tomlinson, G. A. A Molecular Theory of Friction. *Philos. Mag. Ser.* **1929**, *7* (46), 905–939.

(45)   Prandtl, L. Ein Gedankenmodell Zur Kinetischen Theorie Der Festen Korper. *Z. Angew. Math. Mech.* **1928**, *8*, 85–106.

(46)   Tian, K.; Goldsby, D. L.; Carpick, R. W. Rate and State Friction Relation for Nanoscale Contacts: Thermally Activated Prandtl-Tomlinson Model with Chemical Aging. *Phys. Rev. Lett.* **2018**, *120* (18), 186101.

(47)   Wang, L.; McCarthy, T. J. Shear Distortion and Failure of Capillary Bridges. Wetting Information beyond Contact Angle Analysis. *Langmuir* **2013**, *29* (25), 7776–7781.

(48)   Butt, H. J.; Gao, N.; Papadopoulos, P.; Steffen, W.; Kappl, M.; Berger, R. Energy Dissipation of Moving Drops on Superhydrophobic and Superoleophobic Surfaces. *Langmuir* **2016**, *33* (1), 107–116.

For Table of Contents Only

Normal force due to mass

Normal force due to surface tension

solid

Applied Force

Frictional Force, F_f

$F_f = \mu F_N$

γ_{LV} γ_{LV}

Applied Force

θ_F droplet θ_B

Frictional Force, F_f